

Received November 6, 2019, accepted December 1, 2019, date of publication December 16, 2019,  
date of current version December 30, 2019.

Digital Object Identifier 10.1109/ACCESS.2019.2959836

# Attitude Tracking Control Reconfiguration for Space Launch Vehicle With Thrust Loss Fault

YAOKUN ZHANG<sup>ID</sup>, ZHU LI<sup>ID</sup>, ZHONGTAO CHENG<sup>ID</sup>, LEI LIU<sup>ID</sup>,  
AND YONGJI WANG<sup>ID</sup>, (Member, IEEE)

National Key Laboratory of Science and Technology on Multispectral Information Processing, School of Artificial Intelligence and Automation, Huazhong University of Science and Technology, Wuhan 430074, China

Corresponding author: Zhongtao Cheng (ztccheng@hust.edu.cn)

This work was supported by the National Natural Science Foundation of China under Grant 61873319, Grant 61803162, and Grant 61903146.

**ABSTRACT** The thrust loss fault of the space launch vehicle is quite different from that of ordinary actuator efficiency loss. Focusing on the attitude tracking control problem of the launch vehicle with thrust loss fault, the special impacts of that fault on the control system are explored, and a two-stage control reconfiguration strategy based on the cascaded pseudo-inverse allocation method and the neuron adaptive gain scheduling method is proposed for faults with different severity. Meanwhile, a practical reconfigurability analysis for the faulty system based on the control state reachability is presented for some representative fault scenarios. Based on the nonlinear dynamical model of the faulty system, lots of numerical simulations under various fault scenarios are finally carried out. The results indicate that the designed control reconfiguration strategy not only can effectively deal with the thrust loss fault with high practicability but also is easy to implement.

**INDEX TERMS** Space launch vehicle, thrust loss fault, control reconfiguration strategy, cascaded pseudo-inverse allocation, neuron adaptive gain scheduling, reconfigurability analysis.

## I. INTRODUCTION

Space launch vehicle (SLV) is an indispensable vehicle for aerospace activities. Due to its complicated structure and harsh working environment, faults will inevitably occur in it. Literature [1] investigated the launch failure cases of SLV around the world during the period of 1984 to 1994 and showed that the fault of rocket power propulsion subsystem was the most frequent, the most prone and the most harmful fault source. In recent decades, the number of the launch failure case causing by the fault of the rocket power system is still increasing [2]. For examples, in 2012, after the launch of the SpaceX's Falcon 9 carrier rocket in the United States, the thrust of the No. 1 engine was abnormal, and redundant engines were started in time to narrowly avoid a crash accident; in 2017, after the launch of China's CZ-5 launch vehicle, one of the core engines failed to operate normally, which caused the launch mission failed eventually. The control reconfiguration technology for SLV in the presence of a faulty power subsystem is a key way to realize the soft redundancy of SLV, which is of great significance to improve

the reliability and safety of SLV and ensure the success of the launch mission.

At present, the control reconfiguration is generally studied from the perspective of fault-tolerant control (FTC), which has been widely applied to some safety-critical systems, especially in the field of aerospace engineering [3], a large number of FTC methods have been proposed. The most popular ones for control reconfiguration can be roughly divided into the categories as: adaptive control [4]–[6], control allocation [7]–[9], sliding mode control [10]–[12], multi-model switching [13]–[15], and other nonlinear control methods [16]. And the fault types considered in most studies mainly fall on sensor fault, actuator fault and the fault of structural damage. From this point of view, the fault of the power system of SLV belongs to the actuator fault, which can be further divided into some certain types: jammed, floating swing and efficiency loss. Currently, there are a variety of researches on the fault of the jammed or floating rocket servo mechanism [17], [18], while the fault of thruster efficiency loss that referred to as thrust loss fault (TLF) later has been paid less attention to, which is quite different from the fault of rocket servo mechanism or that of ordinary actuator efficiency loss (the widely studied control surface

The associate editor coordinating the review of this manuscript and approving it for publication was Long Cheng.

fault of aircraft [19]–[21], for example). The common adverse impact of TLF of the rocket engine is the reduction of the actuators' efficiency, resulting in slower dynamic response and easier actuator saturation, while its different peculiarities are described in detail as follows:

- 1) First of all, for the programmed guidance that generally used in the design of rocket flight trajectory, the TLF is bound to lead to a considerable deviation between the actual flight path and the predetermined path, in which case, an online reprogramming of flight trajectory is indispensable to generate a new set of attitude control commands to guarantee a successful entry into orbit.
- 2) Secondly, because of the change of flight trajectory in the fault condition, the original flight parameters (such as flight altitude, flight speed, and aerodynamic parameters, etc.) greatly change accordingly resulting in considerable variation of the system model, which makes the controller design and the control parameter tuning based on the nominal model have an unsatisfactory performance or even invalid in some severe fault cases.
- 3) Besides, in a faulty system with TLF, some special external disturbances can be brought into the SLV control system due to the imbalance between different thrusts and the skewing of the SLV's centroid, which will exert tremendous disturbances on the attitude tracking control system.
- 4) The last relevant point worth mentioning is that, as the actuating component of the control system, the rocket engine is more of a crucial component of the power subsystem of SLV, therefore there are many independent and elaborate researches on the fault detection and diagnosis (FDD) technology of the aero-engine [22], [23], which pay more attention to the data-driven methods (statistical analysis or neural networks, etc.) rather than the model-based methods (state or parameter estimation, etc.) using in the conventional FTC systems [3], [24]. Therefore, it is unnecessary to concern too much about how to obtain the fault information to realize an active fault-tolerant control (AFTC), which reduces the difficulty of reconfiguring the control system of SLV to some extent.

In the above analysis, the special impacts of the TLF are presented from the aspects of online updating control commands, uncertain changing control model, considerable external disturbances, and dissimilar fault detection methods, indicating that it is necessary to study the TLF of SLV specifically. Unfortunately, there are few studies to place emphasis on it. Literature [25], [26] focused on the impacts of TLF on the flight path and compared various flight states of SLV before and after TLF in the Matlab/Simulink environment, but did not cover anything about attitude control reconfiguration of the faulty system. Literature [27] utilized the control allocation strategy based on pseudo-inverse and fixed-point methods to reconfigure the attitude control system of SLV when the actuators fail, but the obvious drawbacks

were the neglect of the special impacts of the TLF due to the insufficient analysis of the dynamics of TLF, and the incomplete fault simulation for verification, in which only a less severe fault scenario was simulated. Apart from the problems in the current study mentioned above, to the author's best knowledge, most FTC methods for the over-actuated system are mainly reconfigured from the perspective of control allocation solely [8], [9], [28], namely, the idea of combining multiple reconfiguration methods is rarely applied.

Therefore, focusing on the attitude tracking control system of SLV with TLF, the specific impacts of the TLF on the control system are demonstrated from the perspective of time and frequency domain through dynamics analysis and numerical simulations, and a two-stage control reconfiguration strategy combining the cascaded pseudo-inverse allocation (CPIA) method and the neuron adaptive gain scheduling (NAGS) method is proposed for TLF with different severity from the aspects of the dynamic control allocation and the reconfiguration of controller. Furthermore, by using the concept of state reachability of the control system, a practical idea of reconfigurability analysis for the faulty SLV system is presented for some representative fault scenarios.

The rest of this paper is organized as follows. In section II, the nonlinear dynamical model of a certain SLV is established in consideration of the TLF. In section III, a two-stage control reconfiguration strategy is designed and formulated. And a number of numerical simulations of SLV under different fault scenarios are presented in section IV. Finally, a brief conclusion and future work are summarized in Section V.

## II. DYNAMICAL MODEL OF THE FAULTY SLV

Fig. 1 shows the layout of the SLV's first stage engines from bottom view.  $Ox_b y_b z_b$  is the rocket body coordinate system (CSYS). The four strap-on engines are symmetrically distributed around the rocket on  $y_b$  and  $z_b$  axes in  $Oy_b z_b$  plane and can be used for tangential swing. The two core engines are diagonally distributed in the second and fourth quartiles

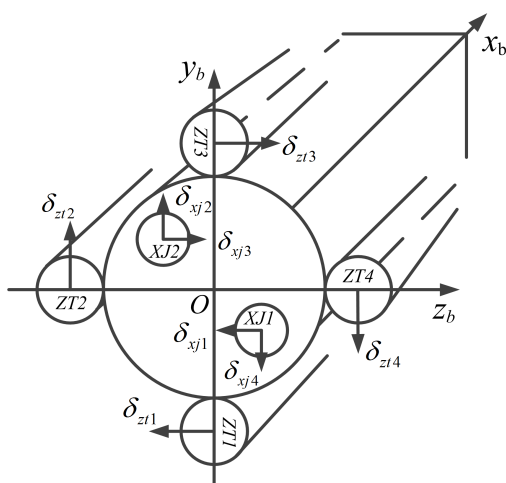


**FIGURE 1.** The bottom view of the engines of a certain SLV.

in  $Oy_bz_b$  plane and can be used for two-way cross swing. The actual oscillation angles of corresponding engines are labeled by  $\delta^{act} = [\delta_{zt1}, \delta_{zt2}, \delta_{zt3}, \delta_{zt4}, \delta_{xj1}, \delta_{xj2}, \delta_{xj3}, \delta_{xj4}]^T$  and the positive direction of each angle is indicated by the arrow shown in the figure [17], [26].

Consider that the actual thrust produced by the faulty engine is proportional to the rated thrust, and then the TLF of the rocket engine can be described by the coefficient matrix  $K = diag\{k_{zt1}, k_{zt2}, k_{zt3}, k_{zt4}, k_{xj1}, k_{xj2}\}$ , in which,  $k_i \in [0, 1]$ , and  $k_i = 0$  and  $k_i = 1$  respectively mean the  $i^{th}$  engine is completely shut down and fault-free, and  $0 < k_i < 1$  means the  $i^{th}$  engine's thrust partly lose. In this way, the thrusts of the faulty engines  $\mathbf{P}^f$  can be given by

$$\mathbf{P}^f = K\mathbf{P} \quad (1)$$

where  $\mathbf{P}^f = [P_{zt1}, P_{zt2}, P_{zt3}, P_{zt4}, P_{xj1}, P_{xj2}]^T$ , and  $\mathbf{P} = [P_{zt}, P_{zt}, P_{zt}, P_{zt}, P_{xj}, P_{xj}]^T$ , in which,  $P_{zt1} \sim P_{xj2}$  are the actual thrusts of the corresponding engines respectively;  $P_{zt}$  and  $P_{xj}$  are the rated thrusts of strap-on engine and core engine at the current moment respectively.

To focus on the impacts of TLF on SLV's dynamical characteristics in the boosting flight phase, the modeling process follows some reasonable assumptions:

- 1) Ignore the rotation of the earth;
- 2) The sloshing of the liquid fuel, the elastic vibration of the rocket body and the wind disturbances are not considered;
- 3) The fault cases involve the leakage of the rocket propellant are not considered;
- 4) The fault cannot be repaired automatically and will last until the end of the flight mission.

According to the Newton's second law and the moment of momentum theorem, and considering the special impacts caused by the TLF, the six DOF rigid body nonlinear dynamical model of the faulty SLV is well deduced:

$$\begin{cases} m\dot{\mathbf{V}} = -\boldsymbol{\omega}_h \times \mathbf{V} + H_B(\mathbf{P}^f + \mathbf{F}_C^f + \mathbf{F}_{ec}^f) \\ \quad + H_A \mathbf{G}^f + H_V(\mathbf{R} + \mathbf{R}_d) \\ \mathbf{J}\dot{\boldsymbol{\Omega}} = -\boldsymbol{\Omega} \times \mathbf{J}\boldsymbol{\Omega} + \mathbf{M}_P^f + \mathbf{M}_C^f + \mathbf{M}_{ec}^f \\ \quad + \mathbf{M}_G^f + \mathbf{M}_R + \mathbf{M}_d \\ \dot{\xi} = \boldsymbol{\Gamma}\boldsymbol{\Omega} \end{cases} \quad (2)$$

where  $m$  is the total mass of the SLV,  $\mathbf{V} = [V_{hx}, V_{hy}, V_{hz}]^T$  is the velocity of the SLV in the half-velocity CSYS;  $\boldsymbol{\omega}_h$  is the rotational angular velocity of the half-velocity CSYS relative to the launch inertial CSYS;  $H_B$ ,  $H_A$  and  $H_V$  are the transformation matrix from rocket body CSYS, launch inertial CSYS, and velocity CSYS to half-velocity CSYS, respectively;  $\boldsymbol{\Omega} = [\omega_{x1}, \omega_{y1}, \omega_{z1}]^T$  is the angular velocity of the rocket body rotating around the center of mass;  $J = diag\{J_x, J_y, J_z\}$  is the moment of inertia matrix;  $\xi = [\varphi, \psi, \gamma]^T$  is the vector of attitude angles (pitch, yaw, roll);  $\boldsymbol{\Gamma}$  is the transformation matrix between the attitude angular velocity and the rotation angular velocity of the rocket body;  $\mathbf{P}^f$ ,  $\mathbf{F}_C^f$ ,  $\mathbf{F}_{ec}^f$ ,  $\mathbf{G}^f$ ,  $\mathbf{R}$ ,  $\mathbf{R}_d$  are the thrust force, control force, eccentric disturbance force, gravity, aerodynamic

force and aerodynamic damping force acting on the rocket body, respectively;  $\mathbf{M}_P^f$ ,  $\mathbf{M}_C^f$ ,  $\mathbf{M}_{ec}^f$ ,  $\mathbf{M}_G^f$ ,  $\mathbf{M}_R$ ,  $\mathbf{M}_d$  are respectively the torques corresponding to the above mentioned forces.

Utilize the small deviation hypothesis to simplify the above dynamical model, and then based on the theory of small perturbation linearization, the linearized dynamical model of the pitch control channel at some selected ballistic feature points can be deduced as (3). (The control of pitch angle is emphatically analyzed since the guidance instruction of the SLV is given by a sequence of varying pitch angles, and the same goes for subsequent analysis.)

$$\begin{cases} \Delta\dot{\theta} = c_1^{\varphi f} \Delta\alpha + c_2^{\varphi f} \Delta\theta + c_3^{\varphi f} \Delta\delta_\varphi + \bar{F}_{Y_1}^f \\ \Delta\ddot{\varphi} = b_1^{\varphi f} \Delta\dot{\varphi} + b_2^{\varphi f} \Delta\alpha + b_3^{\varphi f} \Delta\delta_\varphi + b_4^{\varphi f} \Delta\varphi + \bar{M}_{Z_1}^f \\ \Delta\varphi = \Delta\theta + \Delta\alpha \end{cases} \quad (3)$$

where  $\varphi, \theta, \alpha$  are pitch angle, inclination angle and attack angle, respectively;  $c_1^{\varphi f}, c_2^{\varphi f}, c_3^{\varphi f}, b_1^{\varphi f}, b_2^{\varphi f}, b_3^{\varphi f}, b_4^{\varphi f}$  are linearization coefficients of the pitch control channel under fault condition,  $\bar{F}_{Y_1}^f, \bar{M}_{Z_1}^f$  are the equivalent disturbances.

Notably, in the case of fault, those quantities with superscript  $f$  (such as  $\mathbf{F}^f$ ,  $\mathbf{M}^f$  or  $c_i^{\varphi f}$ , etc.) are related to the fault coefficients  $K$ . For convenience, define the fault influence factors of the strap-on engines and the core engines for three attitude angle control channels as follows:

$$\begin{bmatrix} \rho_{zt\varphi} \\ \rho_{zt\psi} \\ \rho_{zt\gamma} \\ \rho_{xj\varphi} \\ \rho_{xj\psi} \\ \rho_{xj\gamma} \end{bmatrix} = \begin{bmatrix} 0 & -k_{zt2} & 0 & k_{zt4} \\ -k_{zt1} & 0 & k_{zt3} & 0 \\ k_{zt1} & k_{zt2} & k_{zt3} & k_{zt4} \\ 0 & -k_{xj2} & 0 & k_{xj1} \\ -k_{xj1} & 0 & k_{xj2} & 0 \\ k_{xj1} & k_{xj2} & k_{xj2} & k_{xj1} \end{bmatrix} \quad (4)$$

The special forces and torques caused by TLF are analyzed detailedly as follows. First of all, the thrusts of engines that are symmetrically distributed around the rocket cannot cancel each other out if some of them are faulty, which will generate a constant disturbance torque called the unbalanced thrust torque  $\mathbf{M}_P^f$ . The magnitude of  $\mathbf{M}_P^f$  can be determined by (5). It can be known that  $\mathbf{M}_P^f$  crossly acts on the pitch and yaw control channels, but make no difference to the roll control channel.

$$\begin{cases} M_{Px}^f = 0 \\ M_{Py}^f = [\rho_{zt\varphi} P_{zt} r_z, \rho_{xj\varphi} P_{xj} r_x] \mathbf{I} \\ M_{Pz}^f = [\rho_{zt\psi} P_{zt} r_z, \rho_{xj\psi} P_{xj} r_x] \mathbf{I} \end{cases} \quad (5)$$

where  $r_z, r_x$  are the corresponding force arms;  $\mathbf{I} = [1 \dots 1]_{1 \times 8}^T$ .

Secondly, the propellant consumption of the faulty engine is slower than that of other normal working engines, resulting in the mass distribution being no longer symmetrical, which means the location of centroid of the SLV will gradually deviate from the longitudinal axis. Therefore, the eccentric disturbance torque  $\mathbf{M}_{ec}^f$  and the eccentric gravity torque  $\mathbf{M}_G^f$  have to be considered. Assuming the position of the instantaneous center of mass in the rocket body CSYS to be  $\mathbf{r}_{ib}$ ,

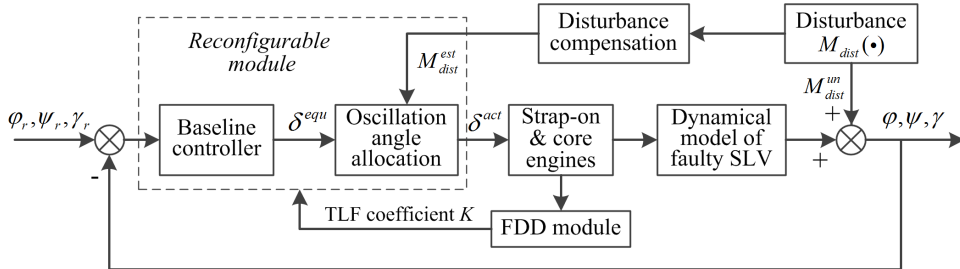


**FIGURE 2.** Schematic diagram of attitude reconfiguration control system of the faulty SLV.

the disturbance torques caused by the centroid skewing can be formulated as (6). Because of the large proportion of the mass of propellant accounts for in the total mass of the SLV, these eccentric torques will be considerable in the severe fault condition.

$$\begin{aligned} \mathbf{M}_{ec}^f &= m \mathbf{r}_{ib} \times \left[ \frac{d\omega_b}{dt} \times \mathbf{r}_{ib} + \omega_b \times (\omega_b \times \mathbf{r}_{ib}) \right] \\ \mathbf{M}_G^f &= \mathbf{r}_{ib} \times \mathbf{G}^f \end{aligned} \quad (6)$$

where  $\omega_b$  is the rotational angular velocity of the rocket body CSYS relative to the launch inertial CSYS.  $\mathbf{r}_{ib} = [0, y_{ib}, z_{ib}]^T$ , which is important for fault analysis, and a estimation method for it is given as follows.

The total mass of the SLV at a certain time can be supposed to consist of the masses of current remaining fuel of each engine  $m_{zt1} \sim m_{zt4}$ ,  $m_{xj1}$ ,  $m_{xj2}$  and the mass of other stationary components  $m_r$ , which is  $m = m_{zt1} + m_{zt2} + m_{zt3} + m_{zt4} + m_{xj1} + m_{xj2} + m_r$ . The fuel consumption flow of the faulty engine  $\dot{m}_c$  is considered to be positively correlated with the thrust, then the residual mass of the faulty engine at any time can be deduced as:

$$\begin{cases} m_{zti} = m_{e0} - \dot{m}_c t_{zti} - \dot{m}_c k_{zti}(t-t_{zti}) & i = 1 \sim 4 \\ m_{xji} = m_{e0} - \dot{m}_c t_{xji} - \dot{m}_c k_{xji}(t-t_{xji}) & i = 1, 2 \end{cases} \quad (7)$$

where  $m_{e0}$  is the initial mass of each engine (we consider the core engine to be the same mass as the strap-on engine), and  $t_{zti}$ ,  $t_{xji}$  are the fault times of each engine, respectively.

Based on the above ideal mass model, the position of the instantaneous center of mass can be estimated easily according to the layout of the rocket engines:

$$\begin{cases} y_{ib} = \frac{1}{m} \left[ d_{zt} (m_{zt3} - m_{zt1}) + \sqrt{2}/2 d_{xj} (m_{xj2} - m_{xj1}) \right] \\ z_{ib} = \frac{1}{m} \left[ d_{zt} (m_{zt4} - m_{zt2}) + \sqrt{2}/2 d_{xj} (m_{xj1} - m_{xj2}) \right] \end{cases} \quad (8)$$

where  $d_{zt}$ ,  $d_{xj}$  are the distances from the center of mass of the strap-on engines and the core engines to the longitudinal axis of the SLV, respectively.

### III. ATTITUDE RECONFIGURATION CONTROL

For the control of the over-actuated system, the control system is generally divided into two relatively independent modules: the baseline controller module for generating virtual

equivalent control commands and the control allocation module for assigning equivalent control commands to every actual actuator. Therefore, the reconfiguration control strategy can be designed from either controller reconfiguration or control reallocation, or both of them.

#### A. CONTROL RECONFIGURATION STRATEGY

The principle of attitude reconfiguration control system of the faulty SLV is shown in Fig. 2. The FDD module observes typical parameters (such as nozzle pressure, turbopump speed, combustor pressure, fuel consumption rate, etc.) during the operation of the engine to identify the fault conditions of engines and obtain the fault coefficient matrix  $K$ , which will be used to reconfigure the faulty system. (As analyzed in the introduction, the detailed implementation process of FDD is beyond the scope of this paper.) Besides, some disturbance torques caused by TLF are estimated and directly introduced into the control allocation process as compensation to eliminate their interference.

Faults with different severity affect the attitude control system differently. When there is no fault, conventional attitude control methods for the SLV, for example, the scheme of selecting a fixed oscillation angle relationship shown in (9) as allocation principle and a PID correction network as baseline controller, can make a good performance.

$$\delta^{equ} = T^0 \delta^{act} = [T_{zt}^0, T_{xj}^0]_{3 \times 8} \delta^{act} \quad (9)$$

where  $\delta^{equ} = [\delta_\varphi, \delta_\psi, \delta_\gamma]^T$  is the equivalent oscillation angle vector.  $T^0$  is the fixed allocation efficiency matrix for the oscillation angles of engines, and  $T_{zt}^0 = 1/4[0, -2, 0, 2; -2, 0, 2, 0; 1, 1, 1, 1]$  is the allocation efficiency matrix of the strap-on engines,  $T_{xj}^0 = 2T_{zt}^0$  is the allocation efficiency matrix of the core engines.

When the TLF occurs, due to the control forces become smaller and unbalanced, the power subsystem will be unable to produce desired control torques by the fixed allocation method, which will result in poor control performance. Therefore, a dynamic oscillation angle allocation method is supposed to be applied firstly according to specific fault situations. Furthermore, as severe faults have great impacts on the dynamical model of the SLV, the control performance under the original controller parameters may still deteriorate even if the virtual angle commands are dynamically assigned.

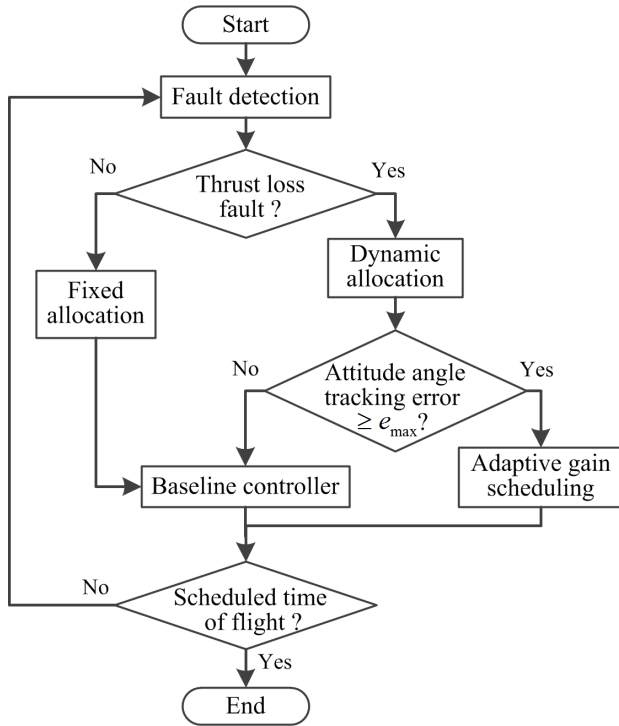


**FIGURE 3.** Schematic diagram of the two-stage control reconfiguration strategy.

In this case, the controller parameters are supposed to be further adjusted adaptively to deal with severe faults. In this way of thinking, a two-stage control reconfiguration strategy shown in Fig. 3 can be naturally got. The work procedure can be described as: if the TLF is detected, the control allocation scheme will be switched from the fixed allocation to the dynamic allocation according to the specific fault condition, and then the attitude angle tracking error is further investigated for whether exceeding the preset acceptable error threshold to determine if it is necessary to use the adaptive tuning parameters generated by the standby controller. This two-stage control reconfiguration strategy implemented step by step according to the fault severity not only reduces the design difficulty of the faulty system but also improves the reliability of the SLV system to some extent.

#### B. CASCADED PSEUDO-INVARIANT ALLOCATION METHOD

The primary objective of the control allocation module is to provide a set of control input to ensure the desired virtual control can be met by the joint working of all the actuators. As for the SLV with TLF, assume the state equation and output equation of the fault-free system to be (10) and that of the faulty system to be (11).

$$\begin{cases} \dot{x} = A^0 x + B^0 \delta^{equ} = A^0 x + B^0 T^0 \delta^{act} \\ \dot{y} = C^0 \dot{x} = C^0 A^0 x + C^0 B^0 T^0 \delta^{act} \end{cases} \quad (10)$$

$$\begin{cases} \dot{x} = A^f x + B^f \delta^{equ} = A^f x + B^f T^f \delta^{act} \\ \dot{y} = C^f \dot{x} = C^f A^f x + C^f B^f T^f \delta^{act} \end{cases} \quad (11)$$

Consider that, for a particular state  $x^*$ , in the fault-free case, the expected oscillation angles outputted by the controller is  $\delta^{act0}$ , and the output of system is  $y^0$ , while in the case of the fault, new oscillation angles  $\delta^{act}$  are wanted to make the output of the faulty system as close as possible to the fault-free system, which is  $y^f \simeq y^0$ . This problem can be described as [7], [29]:

$$\begin{aligned} \min_{\delta^{act}} J &= [(y^f - y^0)^T (y^f - y^0)] / 2 \\ \text{s.t. } |\delta_i^{act}| &< \delta_{max} \end{aligned} \quad (12)$$

where  $\delta_{max}$  is the saturation value of the oscillation angle in the actual system. For the minor faults, the model parameters of the faulty system have little change, which means  $A^f \simeq A^0$ ,  $B^f \simeq B^0$ ,  $C^f \simeq C^0$ . Therefore, the objective function of the above optimization problem is translated to:

$$\min_{\delta^{act}} J = [(T^f \delta^{act} - T^0 \delta^{act0})^T (T^f \delta^{act} - T^0 \delta^{act0})] / 2 \quad (13)$$

Take no account of the saturation of oscillation angle, the (13) has an exact solution:

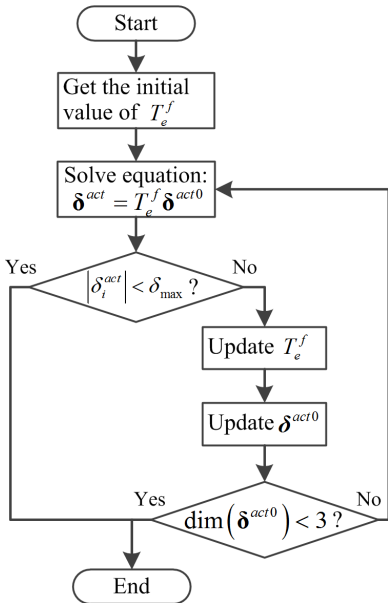
$$\delta^{act} = T_e^f \delta^{act0} = T^{f+} T^0 \delta^{act0} \quad (14)$$

where  $T_e^f$  is called the equivalent allocation efficiency matrix in the case of fault, and  $T^{f+}$  is the pseudo inverse of  $T^f$ . According to the allocation relationship (9), the allocation efficiency matrix of the faulty system can be expressed as  $T^f = [\lambda_{zt} T_{zt}^f, \lambda_{xj} T_{xj}^f]_{3 \times 8}$ , in which,  $T_{zt}^f$  and  $T_{xj}^f$  can be determined by:

$$\begin{aligned} T_{zt}^f &= \left[ \frac{\rho_{zt\varphi}}{k_{zt2} + k_{zt4}}; \frac{\rho_{zt\psi}}{k_{zt1} + k_{zt3}}; \frac{\rho_{zty}}{\sum_{i=1}^4 k_{zti}} \right]_{3 \times 4} \\ T_{xj}^f &= \left[ \frac{\rho_{xj\varphi}}{k_{xj1} + k_{xj2}}; \frac{\rho_{xj\psi}}{k_{xj1} + k_{xj2}}; \frac{\rho_{xjy}}{2(k_{xj1} + k_{xj2})} \right]_{3 \times 4} \end{aligned} \quad (15)$$

and  $\lambda_{zt}, \lambda_{xj}$  are respectively the proportional coefficients of equivalent oscillation angles distributed to the strap-on engines and the core engines, whose optimal values depend on the remaining control capacity of the faulty engines and can be determined by solving the problem  $\min \sum_{i=1}^4 (\delta_{zti} + \delta_{xji})$  if needed.

A cascaded pseudo-inverse allocation (CPIA) method is used for the saturated case [28], [30], whose implementation is shown in Fig. 4. The initial value of  $T_e^f$  is obtained firstly according to the information of the FDD module, and then the oscillation angle of each engine can be obtained by solving allocation formula (14), in which process, the saturated oscillation angles, if any, will be marked and their magnitude will be set as the saturation value, and at the same time the corresponding column in equivalent allocation efficiency matrix  $T_e^f$  and the corresponding term in control variable  $\delta^{act0}$  will be respectively removed. Subsequently, the updated  $T_e^f$  and  $\delta^{act0}$  are used to solve the allocation equation again to obtain the remaining unsaturated oscillation angles. Cycle the process until there is no more saturation or the number of remaining control variables is less than the dimension of the control target.

**FIGURE 4.** Schematic diagram of the CPIA method.

### C. NEURON ADAPTIVE GAIN SCHEDULING METHOD

In the case of the severe fault, the model parameters  $A^f$ ,  $B^f$  and  $C^f$  vary greatly from the normal situation. In order to make the output of the faulty system still similar to that of the normal system by using the same allocation formula (14), the expected oscillation angle  $\delta^{act0}$  is supposed to be adjusted, which means the controller parameters need to be adjusted.

The NAGS method uses the learning law of neural network to adjust the controller parameters online so as to make the system adaptive to different external conditions [31], [32]. The schematic diagram of control reconfiguration based on the NAGS method is shown in Fig. 5. It should be noted that the control allocation is thought to perform ideally enough to integrate into the SLV system for the analysis of controller reconfiguration, which is reasonable in the practical system.

For the incremental PID controller, convert the control error of the closed-loop system  $e(t)$  into a new set of state variables as the inputs of neuron, which is  $\mathbf{X} = [x_1, x_2, x_3]^T = [e(t) - e(t-1), e(t), e(t) - 2e(t-1) + e(t-2)]^T$ . In this way, the synaptic weights of neuron will be respectively corresponding to the proportional, differential and integral coefficients of the controller, which is  $\mathbf{W} = [\omega_1, \omega_2, \omega_3]^T = [k_p, k_i, k_d]^T$ . Select the s-type function (hyperbolic tangent function) as the activation function of the neuron, the output of the neuron can be derived as (16), which can be thought of as equivalent to the output of the PID controller, which means the adjustment of neuronal weights will change the controller parameters accordingly.

$$\begin{cases} u_g(t) = u_{max}(1 - e^{-u(t)})/(1 + e^{-u(t)}) \\ u(t) = u(t-1) + K_u \mathbf{W}^T(t) \mathbf{X}(t) / \|\mathbf{W}\| \end{cases} \quad (16)$$

where  $u(t)$  is the equivalent control variable and  $u_{max}$  is the equivalent control saturation value.

Select  $J(t) = [r(t) - y(t)]^2/2 = e^2(t)/2$  as the performance index function, the updating of neuronal weight  $\Delta\omega_i(t) = \omega_i(t) - \omega_i(t-1)$  can be derived as:

$$\begin{aligned} \Delta\omega_i(t) &= -h_i \frac{\partial J(t)}{\partial \omega_i(t-1)} \\ &= -h_i \frac{\partial J(t)}{\partial y(t)} \frac{\partial y(t)}{\partial u_g(t-1)} \frac{\partial u_g(t-1)}{\partial u(t-1)} \frac{\partial u(t-1)}{\partial \omega_i(t-1)} \end{aligned} \quad (17)$$

where  $h_i$  is the step size. As  $\|\mathbf{W}\| = \sum |\omega_i(t)|$  varies slowly, it is considered to be a constant in the derivation process, and the symbol information  $sgn[\partial y(t)/\partial u_g(t-1)]$  is used to approximate  $\partial y(t)/\partial u_g(t-1)$ . In this way, (17) can be further written as:

$$\begin{aligned} \Delta\omega_i(t) &= h_i e(t) x_i(t-1) sgn \left[ \frac{\partial y(t)}{\partial u_g(t-1)} \right] \\ &\cdot u_{max} [1 - u_g^2(t-1)/u_{max}^2] \end{aligned} \quad (18)$$

According to the above weight adjustment rule, the increment of control error of the closed-loop system  $\Delta e(t) = e(t+1) - e(t)$  can be deduced as:

$$\Delta e(t) = \left( \frac{\partial e(t)}{\partial \mathbf{W}} \right)^T \Delta \mathbf{W} \quad (19)$$

If we set  $\mathbf{Q} = [\partial e/\partial \omega_1, \partial e/\partial \omega_2, \partial e/\partial \omega_3]^T$  and  $\mathbf{H} = diag\{h_1, h_2, h_3\}$ , according to the (17), the above equation can be rewritten as:

$$\Delta e(t) = \left( \frac{\partial e(t)}{\partial \mathbf{W}} \right)^T \mathbf{H} \frac{\partial J(t)}{\partial \mathbf{W}} = -e(t) \mathbf{Q}^T \mathbf{H} \mathbf{Q} \quad (20)$$

In order to analyze the stability of the system, the Lyapunov function  $V(t) = e^2(t)/2$  is selected, and then:

$$\begin{aligned} \Delta V(t) &= e^2(t+1)/2 - e^2(t)/2 \\ &= [2e(t)\Delta e(t) + \Delta e^2(t)]/2 \end{aligned} \quad (21)$$

Substitute (20) into (21), it can be derived that:

$$\Delta V(t) = -\frac{1}{2} [e(t) \mathbf{Q}]^T (2\mathbf{H} - \mathbf{H} \mathbf{Q} \mathbf{Q}^T \mathbf{H}) [e(t) \mathbf{Q}] \quad (22)$$

From the above equation, it can be known that  $\Delta V(t) < 0$  when  $0 < \mathbf{H} < 2(\mathbf{Q} \mathbf{Q}^T)^{-1}$ , in which case the system is closed-loop stable. It indicates that when the step size  $h_i$  is small enough, the control error of the closed-loop system will converge to 0 by using the designed rules of parameter adjustment.

### D. RECONFIGURABILITY ANALYSIS

In order to have a general knowledge of the fault conditions that the system can tolerate in advance, it is necessary to perform a reconfigurability analysis for the system with TLF. The understanding of the system's reconfigurability referred to here is that: under some certain faults, the faulty system always has the available control force to adjust system under the condition of saturation constraints of the actuator during the whole flight process after the occurrence of TLF. It can be described by the control state reachability problem under

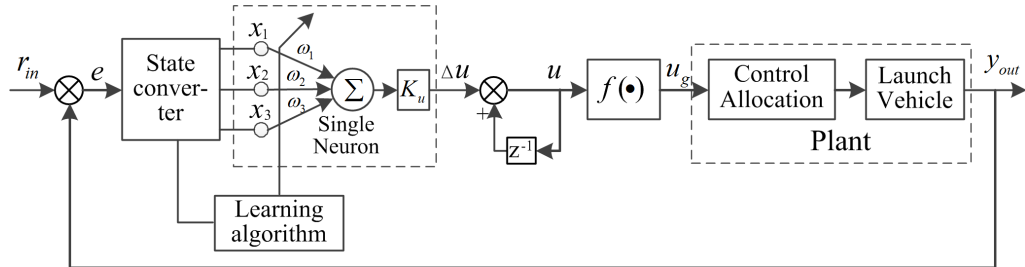


**FIGURE 5.** Schematic diagram of the control reconfiguration based on NAGS method.

constraints as follows. The attitude control system of the SLV can be formulated as a nonlinear dynamic system:

$$\begin{cases} \ddot{x}(t) = f(x(t), \dot{x}(t), \bar{\omega}(t), t) + u(t) \\ x(t_0) = x_0 \\ \|u(t)\| < u_{max} \end{cases} \quad (23)$$

where  $t_0$ ,  $x_0$  is the initial time and state of the system and  $\bar{\omega}(t)$  is equivalent unknown disturbance. Assume  $t_e$  to be the end time of the boosting flight, and then  $t \in [t_0, t_e]$ . Starting from the initial state, the forward reachable set of the system at time  $t_e$  can be defined as:

$$S(t_0, t_e, x_0) = \left\{ \zeta \in \mathbb{R}^n : \exists u(\cdot) \text{ s.t. } x(t_e) \in \zeta \right\} \quad (24)$$

Use  $T_f$  and  $K_f$  to relabel the time of fault occurrence and the value of thrust loss of each engine, which are  $T_f = [t_{z1}, t_{z2}, t_{z3}, t_{z4}, t_{x1}, t_{x2}]^T$  and  $K_f = [k_{z1}, k_{z2}, k_{z3}, k_{z4}, k_{x1}, k_{x2}]^T$ . In the case of fault, use a double element  $\mathbf{a}(T_f, K_f)$  to describe the certain fault, and then the first expression in (23) becomes:

$$\ddot{x}^f(t) = f(x^f(t), \dot{x}^f(t), \bar{\omega}(t), \mathbf{a}, t) + g(T_f, K_f)u(t) \quad (25)$$

In this case, the reachable set of the faulty system becomes:

$$O(t_0, t_e, x_0, T_f, K_f) = \left\{ \zeta \in \mathbb{R}^n : \exists u(\cdot) \text{ s.t. } x^f(t_e) \in \zeta \right\} \quad (26)$$

And it is easy to understand that due to the impacts of the fault, the reachable state range of the system becomes smaller, which means  $O \subsetneq S$ .

Supposing there is no fault or disturbance, the nominal flight state generated according to the guidance commands is  $\zeta_n$ . For a certain fault  $\mathbf{a}_*(T_{f*}, K_{f*})$ , if  $\zeta_n$  is in the reachable set  $O(t_0, t_e, x_0, T_{f*}, K_{f*})$ , which is  $\zeta_n \in O_{\mathbf{a}_*}$ , the faulty system can be considered reconfigurable. According to this definition, in the simple schematic diagram Fig. (6), system with fault  $\mathbf{a}_1$  is reconfigurable, and system with fault  $\mathbf{a}_2$  is unreconfigurable.

Therefore, for a given set of guidance commands, the actual system has a tolerable fault limit, in which case the system reaches its limit of control capability. For the fault at time  $T_{f*}$ , the limit of the fault can be solved by the following optimization problem:

$$\begin{aligned} \min & \|K_f\| \\ \text{s.t. } & \zeta_n \in O(t_0, t_e, x_0, T_{f*}, K_{f*}) \end{aligned} \quad (27)$$

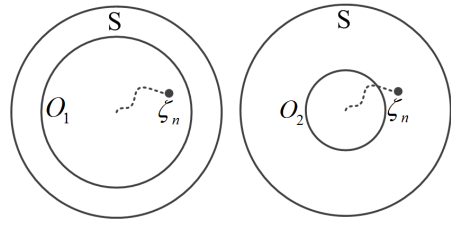


**FIGURE 6.** Schematic diagram of the reconfigurability of faulty systems.

However, it is complicated to directly solve this problem. In fact, it is unnecessary to find the exact value of the fault limit. Therefore, a simple idea is to use the system control  $u(t)$  as a bridge: if the remaining control  $U_r$  of the faulty system is sufficient, the system will definitely reach the desired state following the predetermined commands. Therefore, define  $U_\tau$  is maximum control required by the faulty system at sometime  $\tau$ , the problem (27) can be translated to:

$$\begin{aligned} \min & \|K_f\| \\ \text{s.t. } & U_r(\tau, K_f) \geq U_\tau(K_f) \end{aligned} \quad (28)$$

Since the essence of the control is to generate control torques, the control  $U_\tau$  can be divided into two parts: the control  $U_c$  to maintain angular velocity to follow the angle commands, which is supposed to have a upper bound  $\bar{U}_c$  for the given guidance commands, and the control  $U_d$  to eliminate external disturbances, which can be roughly estimated by the fault model in the second section if ignoring other unknown disturbances. Therefore, a conservative estimate of  $U_\tau$  is finally obtained:

$$U_\tau = \bar{U}_c + U_{dmax} \quad (29)$$

Another thing to consider is that, due to the many attributes of the TLF, such as the type of engine (strap-on or core engine), the position of the engine, the amount of faulty engines, the severity of the fault, etc, the fault conditions in the real system can be extremely complicated. To simplify this problem, it is necessary to select representative faults. Valuable conclusions can be drawn by analyzing the dynamical model (2): the effect of the core engine's fault is of the same properties as the strap-on engine's fault, and the effect of simultaneous fault of multiple engines at any position can be equivalent to the simultaneous fault of two engines at

different control channels. Therefore, the focus can be on the case of a single strap-on engine's fault and the simultaneous fault of two strap-on engines at different control channels (for example, No.1 and No.2 strap-on engines).

#### IV. SIMULATION RESULTS AND ANALYSIS

A simulation platform is built in the VC++6.0 based on the dynamical model of the faulty SLV to simulate the flight under different fault conditions. Simulations are mainly carried out from the following aspects: the simulation analysis for TLF, the CPIA based control reconfiguration, the NAGS based control reconfiguration, and other additional simulations.

##### A. SIMULATION ANALYSIS FOR TLF

According to the reconfigurability analysis method described in III-D, we first figure out the ultimate fault conditions that the system can tolerate. The numerical calculations are carried out on the representative two types of fault, namely, the fault of No. 1 strap-on engine and the simultaneous fault of No. 1 and No. 2 strap-on engines. As predicted, the system has sufficient redundancy for shutdown fault of one engine at any time, while for the simultaneous fault of two engines, the result is shown in Fig. (7), which indicates the relationship between the faults of two engines that the system can withstand ( $k_{zt1}, k_{zt2}$ ) and the time of fault occurrence ( $t_{zt1} = t_{zt2} = t_f$ ). The figure implies that if a serious fault occurs too early, the system will lose its reconfigurability, for examples, the fault of  $k_{zt1} = k_{zt2} = 0.1$  that occurred in the 30s is beyond the reconfiguration capacity of the faulty system, while the system is almost able to cope with the shutdown fault ( $k_{zt1} = k_{zt2} = 0$ ) that occurred after 60s. Although this estimate for the fault severity may be somewhat inaccurate, it still has great reference value. Based on the above simulation results, the time of fault can be set at the middle point (the 80s) of the entire boosting flight phase, which lasts for 160 seconds.

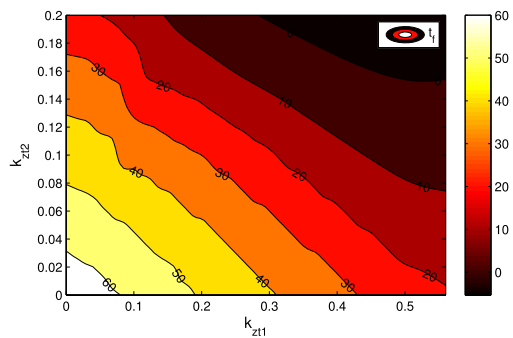


**FIGURE 7.** Reconfigurability analysis result of the simultaneous fault of No.1 and No.2 strap-on engines.

When the thrusts of the faulty engines are reduced by 30%, 60%, and 90% respectively ( $k_{zt1} = k_{zt2} = 0.7, 0.4, 0.1$ ), the special disturbance torques acting on pitch control channel are investigated as shown in Fig. (8), in which, (a), (b), and (c) represent eccentric torques, unbalanced thrust

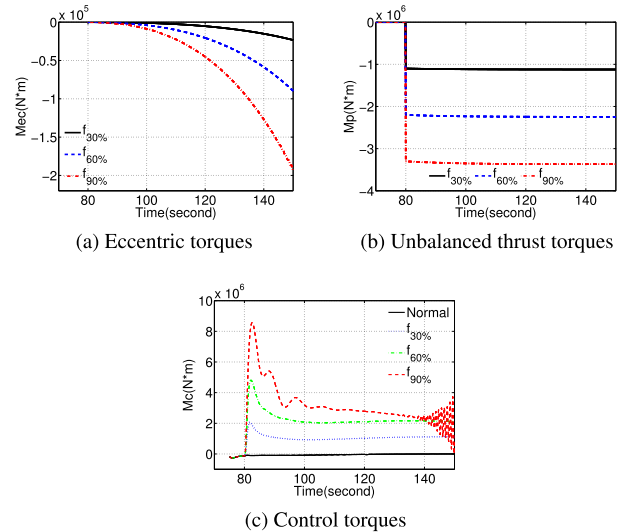


**FIGURE 8.** Torques of the pitch channel under the faults with different severity.

torques, and control torques respectively. It can be seen that the unbalanced thrust torque is a constant disturbance with large amplitude, and the eccentric torque is a time-varying disturbance with nonlinear increase, and the more serious the fault is, the disturbances are greater, which is the main reason for the poor control performance of the faulty system.

##### B. CPIA BASED CONTROL RECONFIGURATION

For the faults of 30%, 60%, and 90%, the curves of the pitch angle tracking error without reconfiguration are shown in Fig. 9. It can be seen that the tracking error is around zero before the TLF occurring, while it does increase sharply to a big level and be adjusted to zero with a very long time when the TLF occurs, and with the extension of the fault acting time, the control errors start to diverge in different degrees in the later stage of the simulation (around 150s), which means that at the time of the fault occurrence, the faulty system without reconfiguration can deal with the fault despite a very poor control performance, however, due to the time-varying of the TLF, the system cannot bear the influences of the fault and start to lose its stability with the extension of the fault

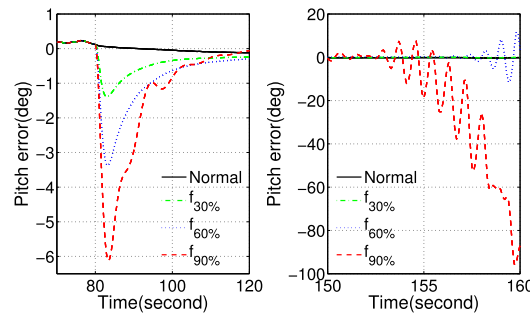


**FIGURE 9.** Pitch errors without reconfiguration.

acting time. It is because of these poor performances that the reconfigurable control is definitely necessary.

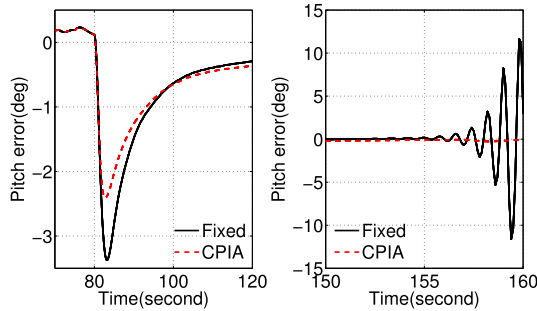


**FIGURE 10.** Pitch errors using the CPIA method under the 60% fault.

Use the CPIA method to reconfigure the control system of 60% fault, and the curves of the tracking error are obtained as shown in Fig. 10, which indicates that the maximum error goes a bit smaller comparing with the original system, and what should be noticed is that the system still maintains its stability in the later stage of the simulation, which is very significant.

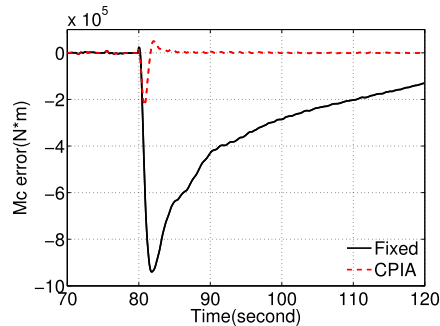


**FIGURE 11.** Comparison of the allocation errors of the control torque.

Moreover, the comparison of the errors between the expected control torque and the actual control torque generated by the engines before and after reconfiguration is presented in Fig. 11 and the comparison of the actual oscillation angles of the strap-on engines before and after reconfiguration are shown in Fig. 12. From these two figures, it can be concluded that for the control system reconfigured by CPIA method, the engines' oscillation angles are properly distributed to meet the expected torque with a smaller oscillation angles, which not only reduces the error between the actual control torque and the expected control torque but also avoids the oscillation angle saturation in some degree, which greatly improves the control performance of the faulty system.

### C. NAGS BASED CONTROL RECONFIGURATION

The pitch angle tracking errors of the reconfigured system using the CPIA method under the faults with different severity are shown in Fig. 13. It can be seen that with the aggravation of the fault severity, the tracking errors of the faulty

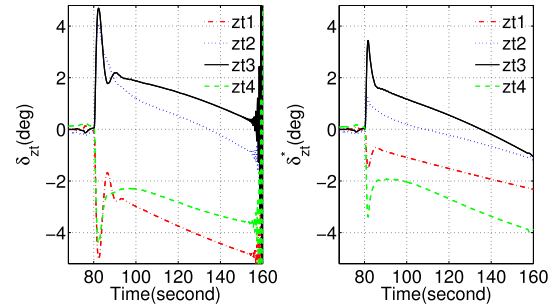


**FIGURE 12.** Comparison of the actual oscillation angles of the strap-on engines before ( $\delta_{zt}$ ) and after ( $\delta_{zt}^*$ ) reconfiguration.

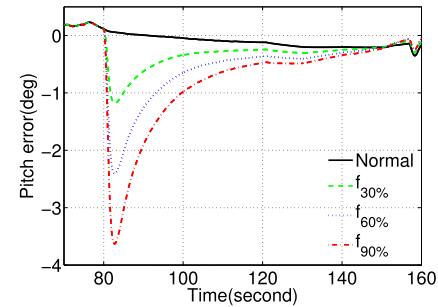


**FIGURE 13.** Pitch errors using the CPIA method under the faults with different severity.

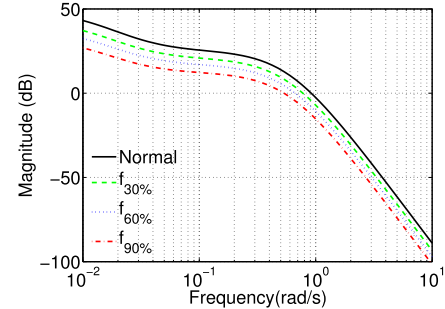


**FIGURE 14.** Amplitude-frequency curves at the feature point of 100s under faults with different severity.

system become larger and the rates of error convergence become slower. For further research, the open-loop frequency characteristics of the SLV with TLF at the ballistic feature point of 100s are investigated, and the amplitude-frequency curves at this feature point are got as shown in Fig. 14, which indicates that the open-loop cut-off frequency of the faulty system reduces gradually with the aggravation of the fault severity, making the system's ability to track commands weaker. Therefore, aiming at the severe fault (90%), the NAGS method is further used to adjust the controller parameters on the basis of the CPIA method, and the simulation results are shown in Fig. 15 and Fig. 16.

As can be seen from Fig. 15, after the control reconfiguration by further using the NAGS method, the adjustment speed of the pitch angle tracking error is significantly accelerated and the tracking error converges to zero quickly even if the

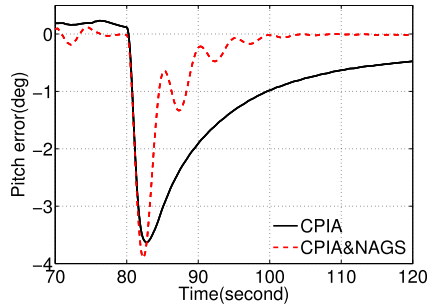


**FIGURE 15.** Pitch errors of the faulty system after adding the NAGS method.

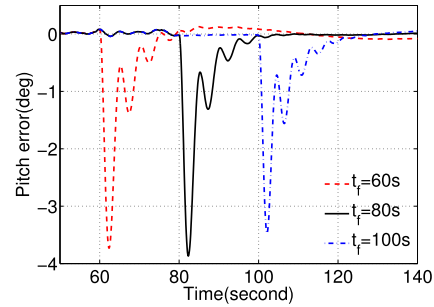


**FIGURE 17.** Pitch errors of the faults with different occurrence times.

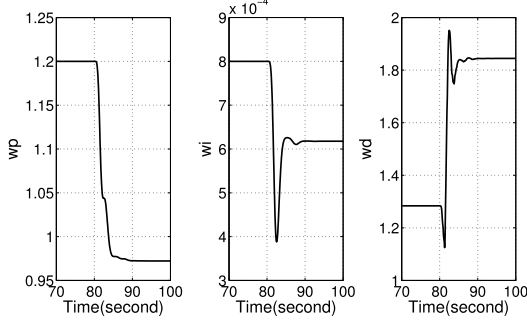


**FIGURE 16.** Adjustment process of the controller parameters.

fault is very serious. And the controller parameters are seen to be adjusted quickly to adapt to the current fault situation as soon as the fault occurs from the process of parameter adjustment as shown in Fig. 16.

#### D. ADDITIONAL SIMULATIONS

On the one hand, the simulated fault scenarios mentioned above mainly revolved around the typical faults with different severity, in order to verify the reconfiguration strategy more comprehensively, some other influencing factors of the TLF are considered:

- 1) According to the reconfigurability analysis of the TLF in III-D, the occurrence time of fault is thought to be a critical factor. Therefore, the 90% faults occurring at the 60s and the 100s are further simulated, and the comparison results are shown in Fig. 17.
- 2) For the running time of the FDD module, the latency time of fault detection has to be concerned inevitably in the real system. Therefore, the 90% faults occurred in the 80s with the latency time of 1s and 1.5s ( $t_d = 1s, 1.5s$ ) are further simulated, and the comparison results are shown in Fig. 18.

From Fig. 17 and Fig. 18, it can be seen that the designed control reconfiguration strategy still performs well for faults with different occurrence times or latency times, which further demonstrates the effectiveness and practicability of this method.

On the other hand, in addition to the method of adaptive adjustment of controller parameters, we try to use the new method from the perspective of system robustness to reduce

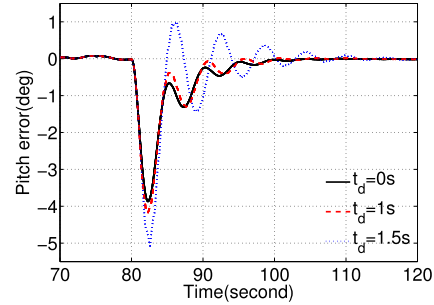


**FIGURE 18.** Pitch errors of the faults with different latency times.

the impacts of fault on the attitude control system. Considering the main impacts of the fault are to generate some special external disturbances and bring about large model uncertainties, the more popular active disturbance rejection controller (ADRC) will be a good choice, which treats all the unfavorable factors as disturbance, and uses an extended state observer to estimate the magnitude of the unknown disturbance so as to compensate for the disturbance using the observations. It has the advantage of independent of accurate control models and resistance to complex disturbances, so it is widely used in some practical engineering systems [33]–[35]. Aiming at the attitude control of the SLV, in the literature [36], an ADR controller based on differential-algebraic approach is designed, which has good fault-tolerant ability for the fault of engines' servo mechanism. Therefore, an anti-disturbance controller based on this method is further used to simulate the faulty system with 90% TLF, and the comparison results of the pitch angle tracking error and the actual oscillation angles of the core engines are shown in Fig. 19 and Fig. 20.

It can be seen that the system using ADRC scheme has a relatively smaller attitude angle error when the fault occurs, indicating that it indeed has a better performance to reject large disturbances, however, the curves of the oscillation angles of the new scheme are not so satisfactory, namely, the oscillation angles change too frequently rather than smoothly, which is a potential hazard to leading a fault of the engines' servo mechanisms. Another disadvantage of ADRC is that its parameters are usually difficult to tune, making it not easy to implement. In contrast, although the system using NAGS scheme has a large error at the moment of the fault,

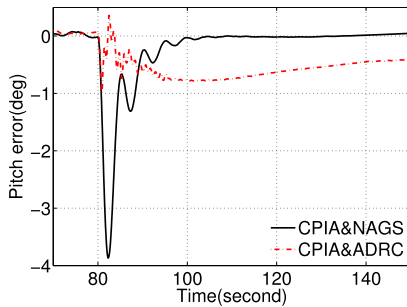


**FIGURE 19.** Comparison of the pitch error of the two control schemes.

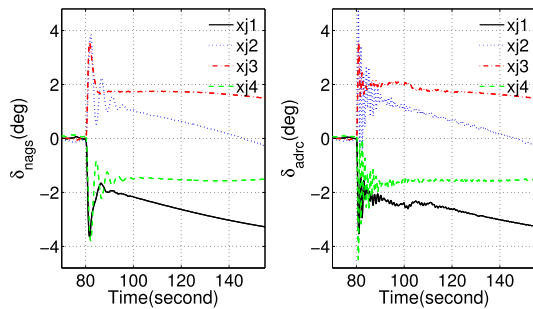


**FIGURE 20.** Comparison of the actual oscillation angles of the two control schemes.

it can be adjusted quickly, and the design and implementation of this scheme are also much simpler.

## V. CONCLUSION

In this paper, some problems with the attitude tracking control of the SLV under TLF are studied. A dynamical model of the faulty SLV was firstly established by analyzing the specific impacts of the TLF, and then a two-stage control reconfiguration strategy based on the cascaded pseudo-inverse allocation method and the neuron adaptive gain scheduling method was proposed for faults with different severity. Afterwards, to figure out the tolerable fault limit of a certain faulty system, a reconfigurability analysis based on the concept of control state reachability was presented for some representative fault scenarios. Finally, through the simulations of the boosting flight process under various fault scenarios, the result of reconfigurability analysis for a specific fault scenario was presented, the internal mechanism of the impact of TLF was parenthetically analyzed, and the effectiveness and practicability of the designed reconfiguration control strategy were also verified by some comparative simulations.

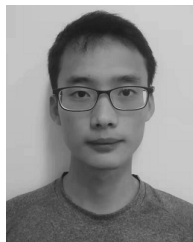
However, there are still some shortcomings in the current research: 1) the CPIA method is not the most effective method to solve the saturation constraint and rate constraint problem existing in practice. Some methods worthy of trial are given in the literature [7], [29], such as the fixed point method; 2) the reconfigurability analysis in this paper shows that the system does not have reconfigurability for some severe faults, the research on how to deal with this situation to avoid system instability is necessary, the tentative solutions

may fall on three aspects: the real-time evaluation of system stability [37], [38], the appropriate adjustment of the thrusts of normal engines to reduce the fault interference and the reprogramming of the flight trajectory to reduce the burden of the control system. These unsolved issues will be studied in the future.

## REFERENCES

- [1] I.-S. Chang, "Investigation of space launch vehicle catastrophic failures," *J. Spacecraft Rockets*, vol. 33, no. 2, pp. 198–205, 1996.
- [2] Z. Zhang, Y. Rong, L. Zheng, and Q. Song, "Redundant propulsion technology for launch vehicle," *Manned Spaceflight*, vol. 19, no. 6, pp. 15–19, 2013.
- [3] S. Yin, B. Xiao, S. X. Ding, and D. Zhou, "A review on recent development of spacecraft attitude fault tolerant control system," *IEEE Trans. Ind. Electron.*, vol. 63, no. 5, pp. 3311–3320, May 2016.
- [4] Q. Shen, C. Yue, C. H. Goh, and D. Wang, "Active fault-tolerant control system design for spacecraft attitude maneuvers with actuator saturation and faults," *IEEE Trans. Ind. Electron.*, vol. 66, no. 5, pp. 3763–3772, May 2019.
- [5] Z. Gao, B. Jiang, P. Shi, J. Liu, and Y. Xu, "Active fault-tolerant tracking control for near-space vehicle attitude dynamics with actuator faults," *Proc. Inst. Mech. Engineers, I, J. Syst. Control Eng.*, vol. 225, no. 3, pp. 413–422, 2011.
- [6] Q. Yang, S. S. Ge, and Y. Sun, "Adaptive actuator fault tolerant control for uncertain nonlinear systems with multiple actuators," *Automatica*, vol. 60, pp. 92–99, Oct. 2015.
- [7] T. A. Johansen and T. I. Fossen, "Control allocation—A survey," *Automatica*, vol. 49, no. 5, pp. 1087–1103, 2013.
- [8] M. E. N. Sørensen, S. Hansen, M. Breivik, and M. Blanke, "Performance comparison of controllers with fault-dependent control allocation for uav's," *J. Intell. Robotic Syst.*, vol. 87, no. 1, pp. 187–207, Jul. 2017.
- [9] Q. Shen, D. Wang, S. Zhu, and E. K. Poh, "Control allocation based fault-tolerant control design for spacecraft attitude tracking," in *Proc. 53rd IEEE Conf. Decis. Control*, Dec. 2014, pp. 4983–4988.
- [10] Y. Zhang, S. Tang, and J. Guo, "Adaptive-gain fast super-twisting sliding mode fault tolerant control for a reusable launch vehicle in reentry phase," *ISA Trans.*, vol. 71, pp. 380–390, Nov. 2017.
- [11] C. Jing, H. Xu, X. Niu, and X. Song, "Adaptive nonsingular terminal sliding mode control for attitude tracking of spacecraft with actuator faults," *IEEE Access*, vol. 7, pp. 31485–31493, 2019.
- [12] X. Yin, B. Wang, L. Liu, and Y. Wang, "Disturbance observer-based gain adaptation high-order sliding mode control of hypersonic vehicles," *Aerospace Sci. Technol.*, vol. 89, pp. 19–30, Jun. 2019.
- [13] B. Jung, Y. Kim, and C. Ha, "Fault tolerant flight control system design using a multiple model adaptive controller," *Proc. Inst. Mech. Eng., G, J. Aerosp. Eng.*, vol. 223, no. 1, pp. 39–50, 2009.
- [14] B. Jung, S.-K. Jeong, D.-H. Lee, and Y. Kim, "Adaptive reconfigurable flight control system using multiple model mode switching," *IFAC Proc. Volumes*, vol. 38, no. 1, pp. 115–120, 2005.
- [15] M. Rodrigues, D. Theilliol, and D. Sauter, "Fault tolerant control design for switched systems," *Anal. Des. Hybrid Syst.*, vol. 39, no. 5, pp. 223–228, 2006.
- [16] X. Lv, B. Jiang, R. Qi, and J. Zhao, "Survey on nonlinear reconfigurable flight control," *J. Syst. Eng. Electron.*, vol. 24, no. 6, pp. 971–983, Dec. 2013.
- [17] L. Liu and Y. Wang, "Control reconfiguration on deadlocked gimbaled thrust of launch vehicle," in *Applied Methods and Techniques for Mechatronic Systems: Modelling, Identification and Control*, L. Liu, Q. Zhu, L. Cheng, Y. Wang, and D. Zhao, Eds. Berlin, Germany: Springer, 2014, pp. 27–59.
- [18] Z. Gao, B. Jiang, P. Shi, and Y. Xu, "Fault-tolerant control for a near space vehicle with a stuck actuator fault based on a takagi-sugeno fuzzy model," *Proc. Inst. Mech. Engineers, I, J. Syst. Control Eng.*, vol. 224, no. 5, pp. 587–598, 2010.
- [19] T. J. J. Lombaerts, Q. P. Chu, J. A. Mulder, and D. A. Joosten, "Modular flight control reconfiguration design and simulation," *Control Eng. Pract.*, vol. 19, no. 6, pp. 540–554, 2011.
- [20] A. Wang, F. Chen, and H. Gong, "Self-healing control for attitude system of hypersonic flight vehicle with body flap faults," *IEEE Access*, vol. 6, pp. 19121–19130, 2018.

- [21] Y. Zhang, V. S. Suresh, B. Jiang, and D. Theilliol, "Reconfigurable control allocation against aircraft control effector failures," in *Proc. IEEE Int. Conf. Control Appl.*, Oct. 2007, pp. 1197–1202.
- [22] F. Lu, J. Jiang, J. Huang, and X. Qiu, "Dual reduced kernel extreme learning machine for aero-engine fault diagnosis," *Aerospace Sci. Technol.*, vol. 71, pp. 742–750, Dec. 2017.
- [23] M. Yuan, Y. Wu, and L. Lin, "Fault diagnosis and remaining useful life estimation of aero engine using LSTM neural network," in *Proc. IEEE Int. Conf. Aircraft Utility Syst. (AUS)*, Oct. 2016, pp. 135–140.
- [24] Z. Gao, C. Cecati, and S. X. Ding, "A survey of fault diagnosis and fault-tolerant techniques—Part I: Fault diagnosis with model-based and signal-based approaches," *IEEE Trans. Ind. Electron.*, vol. 62, no. 6, pp. 3757–3767, Jun. 2015.
- [25] L. Cheng, Y. Cai, L. Mu, and J. Ren, "Fault simulation of launch vehicle flight based on MATLAB/simulink," *Armament Autom.*, vol. 27, no. 9, pp. 8–11, 2008.
- [26] Z. Wang, J. Li, and D. Li, "Failure simulation of thrust decline of launch vehicle based on six dof model," *Manned. Spaceflight*, vol. 23, no. 5, pp. 650–657, 2017.
- [27] P. Huang, Y. Gu, C. Wei, and N. Cui, "Reconfigurable control system design based on control allocation for HLV," in *Proc. 27th Chin. Control Decision Conf. (CCDC)*, May 2015, pp. 3584–3590.
- [28] A. Marks, J. F. Whidborne, and I. Yamamoto, "Control allocation for fault tolerant control of a VTOL otorotor," in *Proc. UKACC Int. Conf. Control*, Sep. 2012, pp. 357–362.
- [29] J. Jin, "Modified pseudoinverse redistribution methods for redundant controls allocation," *J. Guid., Control, Dyn.*, vol. 28, no. 5, pp. 1076–1079, 2005.
- [30] S. Ye, Y. Zhang, X. Wang, and C. A. Rabbath, "Robust fault-tolerant control using on-line control re-allocation with application to aircraft," in *Proc. Amer. Control Conf.*, Jun. 2009, pp. 5534–5539.
- [31] N. Wang, Z. Zheng, and H. Chen, "Model-free PID controller with gain scheduling for turning processes," in *Proc. IEEE Int. Conf. Syst., Man Cybern. Conf. Theme-Syst. Secur. Assurance*, Oct. 2003, vol. 3, pp. 2424–2429.
- [32] Z. Xu and W. Kong, "Design and simulation of single neuron adaptive PID controller," *J. Meas. Sci. Instrum.*, vol. 2, no. 2, pp. 188–190, 2011.
- [33] Y. Yu, H. Wang, and N. Li, "Fault-tolerant control for over-actuated hypersonic reentry vehicle subject to multiple disturbances and actuator faults," *Aerospace Sci. Technol.*, vol. 87, pp. 230–243, Apr. 2019.
- [34] L. Zhou, L. Ma, and J. Wang, "Fault tolerant control for a class of nonlinear system based on active disturbance rejection control and rbf neural networks," in *Proc. 36th Chin. Control Conf. (CCC)*, Jul. 2017, pp. 7321–7326.
- [35] Y. Guo, B. Jiang, and Y. Zhang, "A novel robust attitude control for quadrotor aircraft subject to actuator faults and wind gusts," *IEEE/CAA J. Autom. Sinica*, vol. 5, no. 1, pp. 292–300, Jan. 2018.
- [36] D. Zhao, X. Li, and Y. Wang, "Auto-disturbance-rejection attitude control of carrier rockets using differential algebraic approach," *J. Huazhong Univ. Sci. Technol.*, vol. 39, no. 8, pp. 104–107, 2011.
- [37] L. Liu, S. Dong, Y. J. Wang, and L. L. Ou, "Clearance of flight control law based on structural singular value theory," *IEEE Trans. Aerosp. Electron. Syst.*, vol. 51, no. 3, pp. 2138–2147, Jul. 2015.
- [38] Q. W. Meng, Z. F. Zhong, and J. Z. Liu, "A practical approach of online control performance monitoring," *Chemometrics Intell. Lab. Syst.*, vol. 142, pp. 107–116, Mar. 2015.



**ZHU LI** received the bachelor's degree from the Wuhan University of Science and Technology, in 2018. He is currently pursuing the master's degree with the Huazhong University of Science and Technology. His current research interest includes control allocation and control reconfiguration.



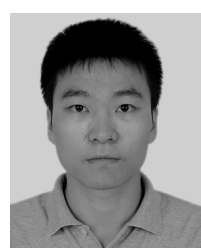
**ZHONGTAO CHENG** received the Ph.D. degree in control theory and control engineering from the Huazhong University of Science and Technology, Wuhan, China, in 2018. He holds a postdoctoral position with the School of Artificial Intelligence and Automation, Huazhong University of Science and Technology. His current research interests include guidance law design, flight control, and cooperative control.



**LEI LIU** received the Ph.D. degree in control theory and control engineering from the Huazhong University of Science and Technology, China, in 2009. He is currently an Associate Professor with the School of Artificial Intelligence and Automation, Huazhong University of Science and Technology. His research interests include guidance and trajectory optimization of aircraft, fault reconfiguration, formation control of multiple UAVs, and flight control.



**YONGJI WANG** received the Ph.D. degree in power plant engineering from the Huazhong University of Science and Technology, China, in 1990. He is currently a Professor with the School of Artificial Intelligence and Automation, Huazhong University of Science and Technology. His research interests include control theory and application, artificial neural networks, system identification, and flight control.



**YAOKUN ZHANG** received the bachelor's degree in detection guidance and control technology from Harbin Engineering University, in 2018. He is currently pursuing the master's degree with the Huazhong University of Science and Technology. His current research interests include intelligent control and artificial neural networks.